J Mater Sci (2007) 42:7214–7219
DOI 10.1007/s10853-007-1611-0

Fabrication and magnetic properties of $NiFe_2O_4$ nanocrystalline nanotubes

Fashen Li · Lijing Song · Dong Zhou · Tao Wang · Ying Wang · Haibo Wang

Received: 24 September 2006 / Accepted: 13 February 2007 / Published online: 10 May 2007

Abstract Aligned $NiFe_2O_4$ polycrystalline nanotubes have been successfully fabricated inside the nanochannels of porous anodic aluminum oxide (AAO) templates by wetting chemical deposition. A mixture of Fe nitrate and Ni nitrate, which was thermally decomposed at no less than 400 °C, was used to yield $NiFe_2O_4$ tubes. By varying the deposition conditions and the parameters of the templates, we could tailor the lengths and the outer as well as the inner diameters of the tubes. Transmission electron microscopy (TEM) images reveal that the nanotubes are uniform and well isolated. X-ray diffraction (XRD) and selected area electron diffraction (SAED) demonstrate that the as-obtained nanotubes can be indexed to polycrystalline cubic spinel. The Mössbauer spectra show that the magnetic hyperfine field is reduced with the decrease of the metrical temperature as well as the decrease of the size of nanoparticles.

Introduction

One-dimensional nanomaterials, such as nanotubes, nanowires, and nanobelts, have been investigated because of their unique electrical, optical, and mechanical characteristics [1–5]. In particular, hollow nanotubes have attracted a great deal of attentions in both fundamental and industrial studies. They possess unique properties that impart them to have potential applications in such fields as electronics, optics, advanced catalysis, and energy storage/conversion. Furthermore, the tubular structure is convenient for the research on the physical and chemical properties of molecules confined in their inner nanospaces and eventually may lead to the mimicking of biological channels**.** After silica nano test tube was reported [6], one important potential application for such nanotubes is as vehicles for delivery of drugs, DNA, proteins, or other biomolecules [7–12] and these vehicles' pathways could be controlled by an external field if the tubular structures are composed of magnetic materials. Therefore, the fabrication technologies of magnetic nanotubes have been developed to fit the above-mentioned application requirements.

Bulk nickel ferrite is a soft magnetic ferrite material with a completely inverse spinel structure. The preparations, magnetic properties, and surface magnetic structures of ultrafine nickel ferrite particles have plenty of outcomes [13, 14], but to our best knowledge few researches about $NiFe_2O_4$ nanotubes have been reported so far. Meanwhile, nanotubes of metals, semiconductors, and polymers are of interest for a broad range of applications, and many approaches have been developed for their fabrications [15]. In fact, template based methods are widely used for preparing nanotubes because they enable good control over their dimensions and can be used to deposit far-flung materials.

In this article, we successfully synthesized tubelike nickel ferrite nanocrystallines in the AAO templates through a simple wetting chemical deposition technique. Owing to its versatility, this approach should be a promising route towards functionalized oxide nanotubes.

F. Li · L. Song (✉) · D. Zhou · T. Wang · Y. Wang · H. Wang
Key Laboratory for Magnetism and Magnetic Materials of Ministry of Education, Lanzhou University, Lanzhou 730000, P.R. China
e-mail: songlj99@yahoo.com.cn

Experiment

Fabrication

The method used here to fabricate the aligned polycrystalline nanotubes is shown schematically in Fig. 1. First, nanoporous AAO templates were prepared by anodic oxidizing of 99.99% pure Al sheet in 5% phosphoric acid solution under a two-step anodizing process (Fig. 1a). By varying the anodization conditions, the pore diameter, spacing, and height can be tuned [16–19], and also the pore ordering can be controlled [20]. The pore diameter of the templates used in this work is about 200–300 nm. Next, $Ni(NO_3)_2 \cdot 6H_2O$ and $Fe(NO_3)_3 \cdot 6H_2O$ were mixed at a molar ratio of about 1:2 to form a nitrate aqueous solution. The AAO templates were put into a vessel containing an appropriate amount of the above-mentioned nitrate solution at 20 °C for about 3 h (Fig. 1b). The loaded templates were cleaned and then fixed on a sample holder, with pores mounted horizontally, and dried in an oven at 60 °C for 24 h. Then a thin Ni/Fe nitrate film covered the pore wall (Fig. 1c). At last, the templates put into a tube furnace annealing at no less than 400 °C for 3 h. During the annealing process, continuous nickel ferrite crystallite films were formed, which led to the formation of aligned $NiFe_2O_4$ polycrystalline nanotubes within the nanopores (Fig. 1d). The two sides of as prepared products were ground using 1000 mesh sand paper before further characterizations. To obtain the TEM images, the samples were dipped into a mixture of 6% H_3PO_4 and 1.8% H_2CrO_4 at 50 °C for 3 h to dissolve the AAO templates completely.

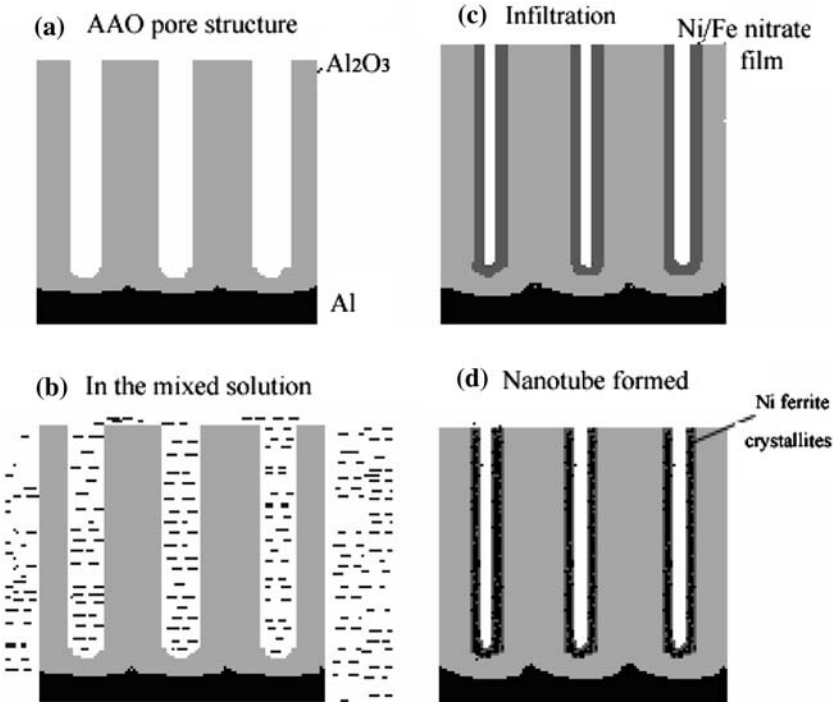

Fig. 1 Fabrication process of aligned $NiFe2O_4$ polycrystalline nanotubes

Measurement

The morphology of the AAO templates was examined by an atomic force microscopy (AFM). A transmission electron microscopy (TEM, Hitachi 600, Japan) was used to characterize the morphology of the nanotubes. The crystalline structures of the samples were obtained by X-ray diffractometer (XRD, Philips X'Pert, Holland; Cu Kα radiation, $\lambda = 1.54056$ Å) and was identified according to JCPDS. The atomic absorption spectroscopy (AAS) analysis gave an atomic ratio of Fe:Ni of the nanotubes. Macroscopic magnetic properties of the samples at room temperature were tested by a vibrating sample magnetometer (VSM, Lakeshore 7304, USA). Mössbauer spectra were taken by a constant acceleration transmission Mössbauer spectrometer equipped with ^{57}Co (Pd). Using α-Fe to calibrate the maximum speed of the spectrometer, the spectra parameters were calculated by fitting Lorentzian line shapes to the experimental data by least-squared method.

Results and discussion

Morphology and structure

For AAO template, its micrograph was investigated by AFM. The results indicate that the diameters and inter-pore distances (center to center) are about 200–250 and 300–350 nm, respectively (see in Fig. 2). If the template is of monodisperse size distribution, aligned or ordered, so are

the nanotubes, and ordered ferrite nanotube array can be obtained if the template is removed. Fig. 3 shows TEM images of $NiFe_2O_4$ nanotubes with about 200–300 nm in diameter, which correspond to that of pores of AAO template, and 10 nm in wall thickness. It can be seen that the nanotubes prepared by AAO template synthesis are of regular size and continuous. The inset of Fig. 3b shows the result from selected area electron diffraction (SAED) that focused on the end of a nanotube of the same sample, which demonstrates clearly that the rings belong to the nickel ferrite phase and correspond to the diffraction of (220) and (311). The AAS analysis indicates that the atomic ratio of Fe:Ni of the nanotubes is 2:1.

Figure 4 shows the X-ray diffraction (XRD) patterns of the $NiFe_2O_4$ nanotubes after annealing. We can see in Fig. 4a that 400 °C was sufficient to the complete formation of nickel ferrite crystalline phase with cubic spinel structure. Generally, the grain size of nanomaterial grows distinctly with the increase of the annealing temperature. Whereas, in this case, the average grain sizes estimated by Scherrer's formula are about 9 nm annealed at 500 °C and 10 nm annealed at 600 °C, respectively. It is found that the walls of the nanotubes can greatly limit the increase of the nano grains. The templates are dipped in the solutions with the same time, so the thickness of the walls are almost same even under different annealing temperatures and the grains of the wall also have similar sizes. However, as seen in Fig. 4 the intensities of all peaks become stronger and the widths of the peaks decrease with the increase of the annealing temperature, which show that the crystallization improves and the grain size becomes larger.

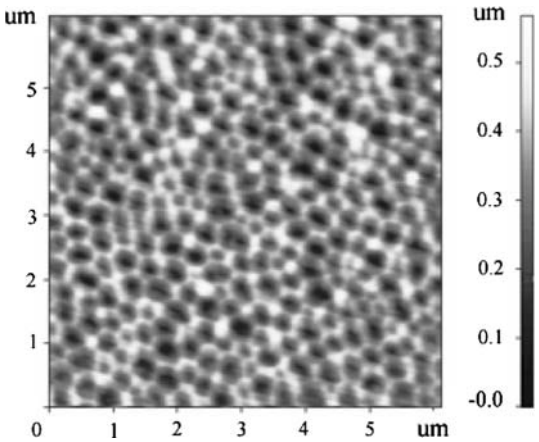

Fig. 2 AFM image of the AAO template

Magnetic properties

Figure 5a presents the transmission Mössbauer spectra (MS) of the samples annealed under various temperatures and measured at room temperature, and the incident γ rays are parallel to the long axes of nanotubes (perpendicular to the AAO membrane). The Mössbauer spectrum of the sample annealed at 600 °C is fitted by magnetic splitting sextets and a doublet. With decreasing the annealing temperatures, the doublet becomes stronger and there is only a doublet when the sample is annealed at 400 °C.

For conventional $NiFe_2O_4$ crystal, the Mössbauer spectrum is usually fitted by two sextets corresponding to the resonance absorptions of iron nuclei which reside in the octahedral (*B*) and tetrahedral (*A*) sites, and the main reason for magnetic splitting sextets below the Curie temperature (590 °C) is the splits of nuclear magnetic energy level caused by a strong antiferromagnetic superexchange interaction between metal ions in the lattice. Furthermore, for nanomaterial, the doublet of the spectra comes primarily from superparamagnetic relaxation caused by small size effect.

For the sample annealed at 400 °C, there is only a doublet because the sizes of the grains may be too small to restrain the thermal fluctuations. Owing to a wide grains size distribution, both the samples that treated at 500 and 600 °C include some grains which are smaller than the critical size, and the superparamagnetic doublets can be induced. Besides the normal sextets, the spectra are broadened seriously, and another sextet is presented for the contribution of the resonance absorption of the interface

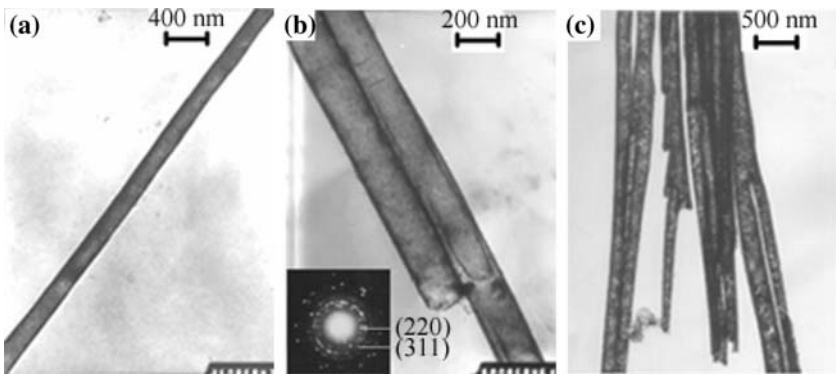

Fig. 3 TEM images of (**a**) a single $NiFe_2O_4$ nanotube annealed at 400 °C, (**b**) two paratactic $NiFe_2O_4$ nanotubes annealed at 500 °C and select area electron diffraction (inset), which focused on the end of the nanotube, showing rings that match the d-spacing for the spinel structure, (**c**) a bunch of $NiFe_2O_4$ nanotubes annealed at 600 °C, with about 200 nm in diameter

and surface iron nuclei (*I*). Therefore, each spectrum can be interpreted as three sextets and one doublet. With the increment of the annealing temperature, it is obvious that the areas of the sextets are enhanced.

For the sample annealed at 600 °C, Mössbauer measurement was also taken at a tempreture of 80 K shown in Fig. 5b, in which the doublet of the spectrum disappears. A superparamagnetic relaxation of the small size grains in the polycrystalline nanotubes is involved in the thermally activated process, by which the doublet is affected, suggesting that the thermal fluctuations play a vital role in the magnetic properties of the nickel ferrite nanotubes. Table 1 shows the ^{57}Fe Mössbauer parameters deduced from the Mössbauer spectra of the samples. The site *A*, *B* and *I* refer to iron nuclei reside in the octahedral sites, tetrahedral sites as well as the interface and surface sites of nanotubes. The Q.S. and H_{hf} represent the quadrupole splitting and the hyperfine magnetic field of the aligned $NiFe_2O_4$ polycrystalline nanotubes. As can be seen, the smaller the size of the grains is, the lower the hyperfine field is. It is also found that the hyperfine field is reduced with the decrease of measuring temperature. These can be explained by the collective magnetic excitations [21]. In this theory, the magnetic moments of small size grains fluctuate around an equilibrium position because of thermal disturbances and then the average hyperfine magnetic field can be expressed as:

$$H_{hf}(V, T) = H_{hf}(V = \infty, T) < \cos\theta >_T \quad (1)$$

H_{hf} ($V = \infty$, T) is the H_{hf} of bulk sample, V is the volume of a particle, $<\cos\theta>_T$ is the average cosine value of the angle between the magnetization and the easy magnetizing axis, and

$$< \cos\theta >_T \approx 1 - k_B T/2KV \quad (2)$$

where k_B is Boltzmann constant, and K is the effective anisotropy constant of the particle**.** Compared with the iron nuclei inside the grains of the tubes, the surface and interfacial iron nuclei have less H_{hf}, which indicates that there are smaller extranuclear electron density, longer distance among atoms and lower symmetry in those iron

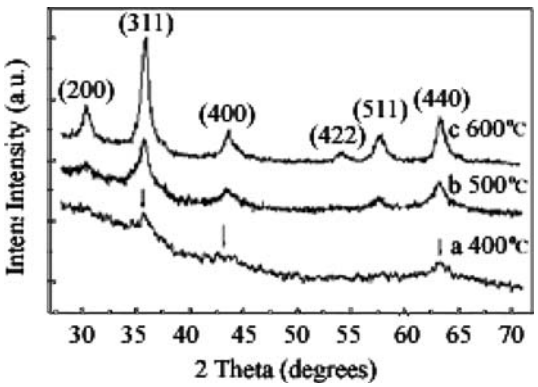

Fig. 4 X-ray diffraction patterns of the $NiFe_2O_4$ nanotubes with AAO templates: sample (**a**) annealed at 400 °C for 3 h, sample (**b**) annealed at 500 °C for 3 h, sample (**c**) annealed at 600 °C for 3 h

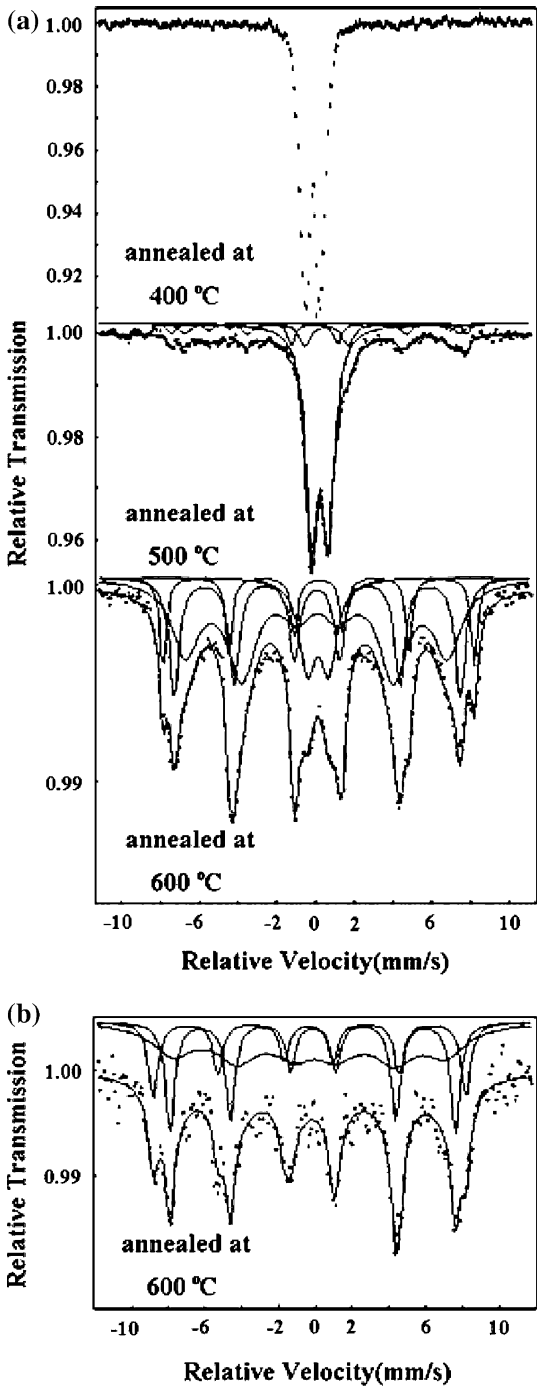

Fig. 5 (**a**) Room temperature transmission Mössbauer spectrum (MS) of the samples annealed at 400, 500 and 600 °C, (**b**) MS of sample annealed at 600 °C taken at 80 K

Table 1 Parameters deduced from the Mössbauer spectra of the samples: the site refers to the iron nuclei which reside in the octahedral sites (*B*), tetrahedral sites (*A*) as well as interfacial and surface sites of the nanotubes (*I*); the Q.S. and H_{hf} represent the quadrupole splitting and the hyperfine magnetic field of $NiFe_2O_4$ nanotubes, respectively

Sample	Measurement temperature	Site	Q.S./ mm s^{-1}	H_{hf} (*T*)
Annealed at 500 °C	RT	*A*	–0.11	44.24
		B	0.11	47.46
		I	0.44	38.68
Annealed at 600 °C	RT	*A*	0.01	46.02
		B	–0.01	50.11
		I	–0.02	42.17
Annealed at 600 °C	80 K	*A*	–0.00	48.53
		B	0.03	53.15
		I	–0.16	46.36

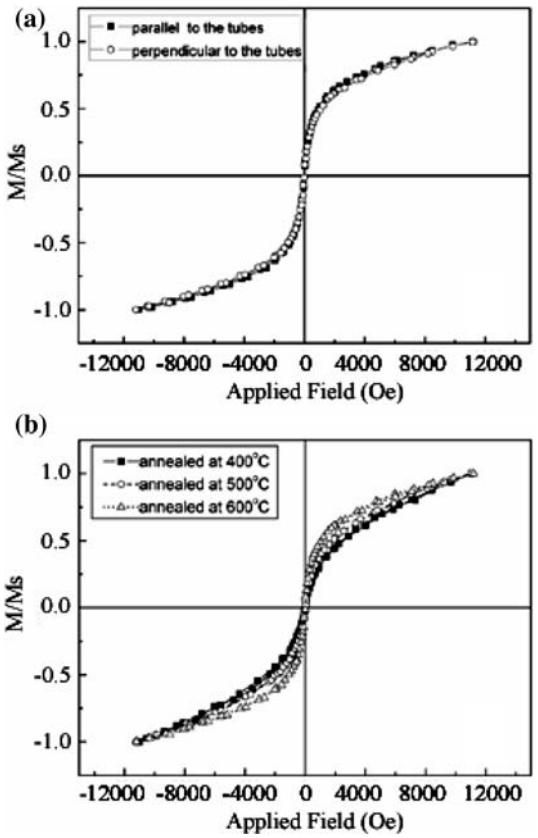

Fig. 6 The magnetization hysteresis loops at room temperature: (**a**) the 600 °C treated sample (parallel to the tubes means the applied field is parallel to the length axis of nanotubes; perpendicular to the tubes means field perpendicular to the length axis of nanotubes), (**b**) hysteresis loops of the samples annealed at 400, 500 and 600 °C, with the applied field parallel to the length axis of the nanotubes

atoms. And a broaden sextet also shows that there is a continuum of iron atom states.

In Mössbauer measurements, the angle (θ) between the incident γ rays and the magnetization direction can be assessed by the relative intensity ratio:

$$I_{2,5}/I_{1,6} = 4\sin^2\theta/3(1+\cos^2\theta) \quad (3)$$

where $I_{2,5}$ and $I_{1,6}$ are the relative intensities of the 2, 5 and 1, 6 peaks in magnetic splitting sextets. When the magnetic moments of the ^{57}Fe atoms in the sample are arrayed disorderedly, the intensity ratio of the 2, 5 and 1, 6 peaks is 2/3. The relative intensity ratio $I_{2,5}/I_{1,6}$ we got from Fig. 5b is about 2/3, so it is deduced that the distributions of the magnetic moments in the sample are random and do not have preferred orientations.

Figure 6 shows the room temperature magnetization hysteresis loops of prepared aligned $NiFe_2O_4$ polycrystalline nanotubes, with the external field applied parallel and perpendicular to the long axis of the tubes. No obvious preferred orientation is observed (Fig. 6a) in this tubular material. However, it can be seen that the superparamagnetic phase decreases with the increase of the grain size, and the coercivity (H_c) is also enhanced with the improvement of crystallization (Fig. 6b).

Conclusion

To summarize, $NiFe_2O_4$ polycrystalline nanotubes have been prepared within the nanochannels of AAO templates by a simple method. It is indicated that the nanotubes are of cubic spinel structure with 200–300 nm in diameter and 2 μm in length. Based on the results of the Mössbauer measurements and analysis, a surface and interface iron atoms phase is of presence in these ferrite tubules and magnetic hyperfine fields of the samples are also discussed. It is found that the doublets are resulted from superparamagnetic effect, which caused by the small size grains in the sample annealed at 600 °C. With the increase of annealing temperature, H_c is also increased. The study of the nanotubes leads to striking and yet fairly understood differences from the better-known nanowire arrays.

Acknowledgements This work was supported by the National Natural Science Foundation of China, No.90505007.

References

1. Iijima S (1991) Nature 354:56
2. Hu J, Odom TW, Lieber CM (1999) Acc Chem Res 32:435
3. Han WQ, Fan S, Li Q, Hu Y (1997) Science 277:1287
4. Pan ZW, Dai ZR, Wang ZL (2001) Science 291:1947

5. Wang ZL (2004) Annu Rev Phys Chem 55:159
6. Gasparac R, Kohli P, Mota MO, Trofin L, Martin CR (2004) Nano Lett 4:513
7. Chang TMS, Prakash S (2001) Mol Biotech 17:249
8. Allen C, Maysinger D, Eisenberg A (1999) Colloids Surf B 16:3
9. Ulrich KE, Cannizzaro SM, Langer RS, Shakeshelf KM (1999) Chem Rev 99:3181
10. Soppimath KS, Aminabhavi TM, Kulkarni AR, Rudzinski WE (2001) J Contol Release 70:1
11. Thurmond KB, Huang H, Clark CG., Kowalewski T, Wooley K (1999) Colloids Surf 16:45
12. Langer R (1990) Science 249:1527
13. Pannaparayil T, Marande R, Komarneni S, Sankar SG. (1988) J Appl Phys 64:5641
14. Morrish AH, Haneda K (1981) J Appl Phys 52:2496
15. Xia YN, Yang PD, Sun YG, Wu YY, Mayers B, Gates B, Yin YD, Kim F, Yan YQ (2003) Adv Mater 15:353
16. O'Sullivan JP, Wood GC (1970) Proc R Soc Lond Ser A 317:511
17. Masuda H, Fukuda K (1995) Science 268:1466
18. Jessensky O, Muller F, Gosele U (1998) Appl Phys Lett 72:1173
19. Li AP, Muller F, Birner A, Nielsch K, Gosele U (1998) J Appl Phys 84:6023
20. Masuda H, Yamada H, Satoh M, Asoh H, Nakao M (1997) Appl Phys Lett 71:2770
21. Mørup S (1983) J Magn Magn Mater 37:139